8 ^{27}Al and ^{23}Na Chemical Shielding Anisotropies

Traditionally only the heavier quadrupolar nuclei are considered to be influenced by the combined effect of quadrupole coupling and CSA. However, with todays high magnetic field strengths (approaching 21 T) the spectral effects of the *small* anisotropic shieldings for the lighter quadrupoles become more visible.

This chapter reports the first convincing observation and quantitation of ^{27}Al and ^{23}Na CSA's. The materials investigated are α-Al_2O_3, $NaNO_3$, and Na_2SO_4, for which the quadrupole coupling parameters are well-known (*7*, *70*, *71*, *74*, *142*, *169–171*).

8.1 ^{27}Al Chemical Shielding Anisotropy

Despite the numerous solid-state ^{27}Al NMR studies in the literature, little attention has been paid to the possibility of the CSA appearing as an additional ^{27}Al solid-state NMR interaction to the quadrupole coupling. No evidence for the existence of ^{27}Al CSA's has come from the many ^{27}Al MAS studies (where it may easily be averaged). Still, there has been an ongoing dispute concerning the possible existence of small ^{27}Al CSA's. Recent observations of ^{71}Ga CSA's in inorganic solids (*79*, *94*) give further support to the this assumption.

In some of the numerous ^{27}Al NMR studies presented in the literature the experimental spectra could only be properly simulated when the CSA interaction was considered in addition to the quadrupole coupling (*114*, *172*). This section describes an ^{27}Al single-crystal NMR study of α-Al_2O_3 which we believe represents the first clearcut determination of an ^{27}Al CSA. Following our work (*56*) there have been

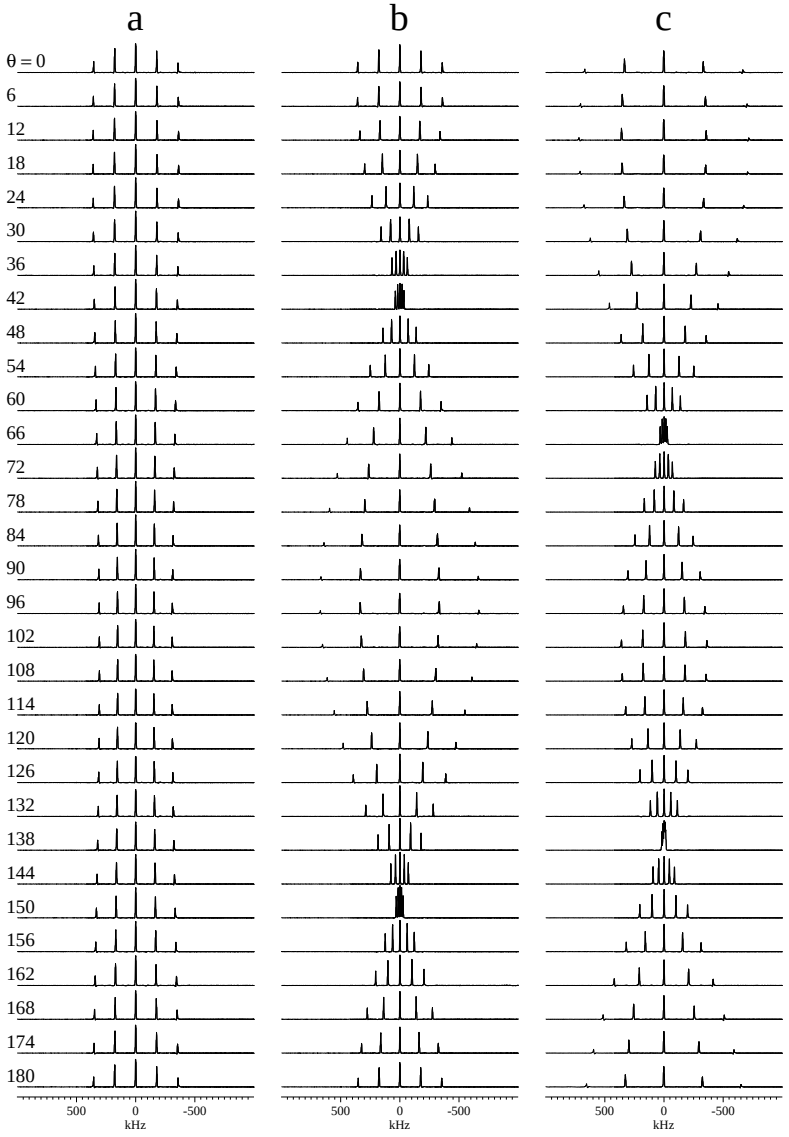

Figure 8.1: ^{27}Al single-crystal NMR spectra of α-Al_2O_3 each recorded following a 6° increment in the rotation about the $-x^{\mathrm{T}}$ (a), y^{T} (b), and $-z^{\mathrm{T}}$ (c) axis.

other ^{27}Al solid-state NMR studies reporting the observation of ^{27}Al CSA's (*108*).

^{27}Al Single-Crystal NMR of α-Al_2O_3

Figure 8.1 shows the ^{27}Al NMR spectra of a crystal of α-Al_2O_3 (size $1 \times 5 \times 5$ mm^3) recorded employing the three-axis goniometer single-crystal NMR probe.[1] The total time required for acquisition of all 93 spectra is less than 4 hours. For

[1]The spectra are recorded at 9.4 T (104.2 MHz) employing single-pulse excitation ($\tau_{\mathrm{p}} = 0.3$ μs for $\gamma B_1/2\pi \approx 50$ kHz), a spectral width of 2 MHz, and 128 scans with a repetition delay of 1 s. Each spectrum is followed by an incrementation in the rotation angle of 6°.

all spectra five distinct resonances corresponding to the five ^{27}Al single-quantum transitions are observed and have linewidths of 3-8 kHz. In some cases a doublet-like lineshape is observed and is ascribed to homonuclear dipole couplings caused by the short distances to the neighboring aluminum nuclei (each aluminum nucleus is surrounded by four other aluminum nuclei with distances between 2.66 and 2.79 Å (*155*, *156*)).

The rotation plots for the ^{27}Al satellite transitions are shown in fig. 8.2a-c where the experimental resonances are marked as dotted circles. These resonances are dominated by the first-order quadrupolar Hamiltonian, and the rotation plots may therefore be used to determine the quadrupole coupling parameters. The solid lines in the rotation plots correspond to the optimized quadrupole coupling parameters which are summarized in table 8.1 including error limits (95% confidence intervals). We note that the quadrupole coupling parameters are in excellent agreement with those of previous studies (*7*, *71*, *74*, *169–171*).

The rotation plots for the central transition frequencies are shown in fig. 8.2d-f where dotted circles represent the center of gravity for the quite broad resonances observed for this transition. Simulations of these rotation plots employing the quadrupole coupling parameters determined from the satellite transitions (table 8.1) for calculation of the second-order quadrupolar shift and optimization of the isotropic chemical shift only, are shown as the dashed lines in fig. 8.2d-f. It is obvious that the experimental resonance frequencies do not agree with the simulations including the quadrupole coupling only. However, when the CSA is included in the simulation, the solid lines in fig. 8.2d-f are obtained. These simulations employ the quadrupole coupling parameters determined from the satellite transitions and the optimized parameters for the ^{27}Al CSA ($\delta_\sigma, \eta_\sigma$), isotropic chemical shift (δ_{iso}), and relative orientation of the quadrupole coupling and CSA tensors (χ, the Euler angles ψ and ξ become undefined when the tensors are axially symmetric) as listed in table 8.1.

α-Al_2O_3 belongs to the hexagonal spacegroup $R\overline{3}c$ and with the aluminum nuclei

Table 8.1: ^{27}Al quadrupole coupling ($C_{\mathrm{Q}}, \eta_{\mathrm{Q}}$) and CSA ($\delta_\sigma, \eta_\sigma$) parameters, isotropic chemical shift (δ_{iso}), and relative orientation (χ) of the σ_{zz} and V_{zz} principal elements for α-Al_2O_3.

Method	C_{Q} [MHz]	η_{Q}	$\delta_{\mathrm{iso}}{}^{a}$ [ppm]	δ_σ [ppm]	η_σ	χ [°]	Reference
SC[b]	2.403 ± 0.015	0.009 ± 0.013	18.8 ± 0.3	-17.3 ± 0.6	0.03 ± 0.06	2.7 ± 1.6	This work
SC	2.393	0[c]	–	–	–	–	*71*
MAS	2.38 ± 0.01	0.00 ± 0.02	16.0 ± 0.2	–	–	–	*7, 74*
SQUID	2.39 ± 0.01	0[c]	–	–	–	–	*169*
NQR[d]	2.389 ± 0.002	0.091 ± 0.007[e]	–	–	–	–	*170*
SC	2.4031 ± 0.0002	0[c]	–	–	–	–	*171*

[a] Isotropic chemical shifts are relative to a 1.0 M solution of $AlCl_3$. [b] Single-crystal NMR from our laboratory employing the three-axis goniometer probe (*56*). [c] Axial symmetry ($\eta_{\mathrm{Q}} = 0$) assumed from crystal symmetry. [d] Study performed at 77 K. [e] The deviation from $\eta_{\mathrm{Q}} = 0$ has previously been discussed (*7, 74*).

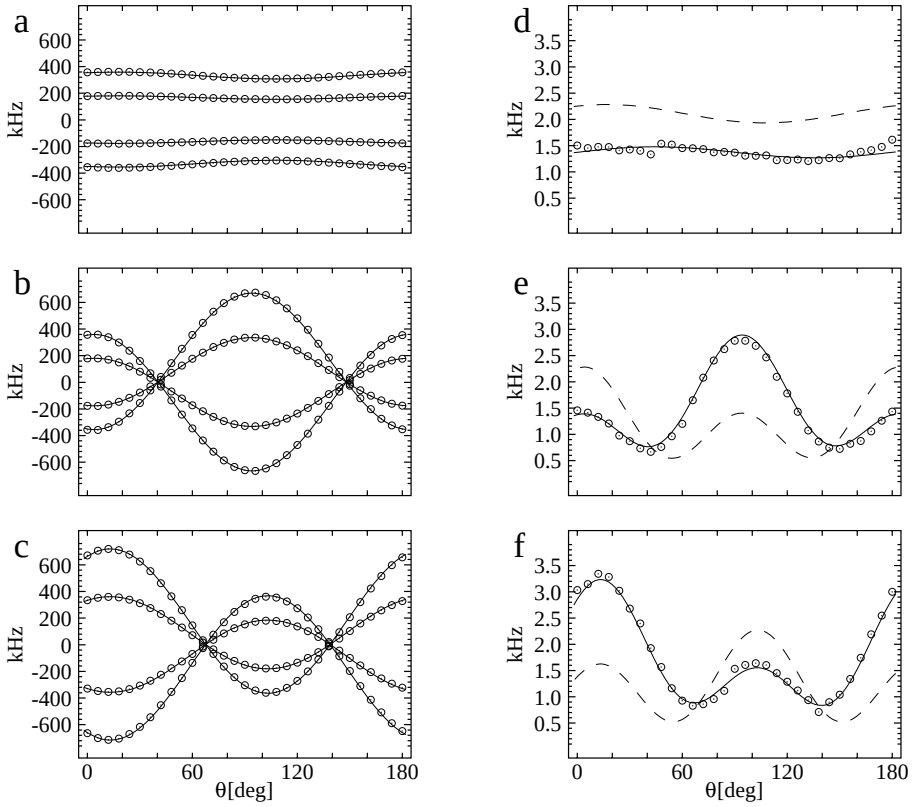

Figure 8.2: Rotation plots for the ^{27}Al satellites (a-c) and central transition (d-f) for rotation about the $-x^{\mathrm{T}}$ (a, d), y^{T} (b, e), and $-z^{\mathrm{T}}$ (c, f) axis. The experimental resonances are marked as dotted circles and the solid curves are calculated using the optimized parameters given in table 8.1. The dashed lines in (d-f) represent calculations including only the quadrupole coupling parameters and optimized isotropic chemical shift.

located in position 12(c) with local $\overline{3}$ symmetry (*155*, *156*). Thus, the V_{zz} and σ_{zz} elements should be aligned along this axis (i.e., these two principal elements should be parallel implying that $\chi = 0°$) and the two tensors should be axially symmetric ($\eta_\lambda = 0$). The axial symmetry is fulfilled within the error limits for both the quadrupole coupling and CSA tensors, and the Euler angle $\chi = 2.7 \pm 1.5°$ indicates that the σ_{zz} and V_{zz} elements are approximately parallel.

In conclusion, we have determined the ^{27}Al quadrupole coupling and CSA parameters for α-Al_2O_3. All parameters are determined with a high degree of precision and clearly demonstrate the presence of ^{27}Al CSA. The parameters conform to the crystal symmetry of α-Al_2O_3 which supports the reliability of the parameters.

8.2 ^{23}Na Chemical Shielding Anisotropy

It appears that the only report on ^{23}Na CSA is an old single-crystal NMR study of $NaNO_3$, $NaClO_3$, and $NaBrO_3$ performed at very low magnetic field stengths (1.0 and 5.8 T). However, in more recent ^{23}Na MAS studies of Na_2SO_4 the authors have reported on spectral effects which could not be simulated by the quadrupole coupling interaction only (*173*, *174*). Thus, these effects were ascribed to the ^{23}Na CSA, although there were no attempts to quantify this interaction.

^{23}Na Single-Crystal NMR of $NaNO_3$

Prompted by the observation of ^{27}Al CSA in α-Al_2O_3 I decided to analyze the rotation plots for the central transition resonances of ^{23}Na in $NaNO_3$ for determination of a possible ^{23}Na CSA. To enhance the spectral effect of the shielding interaction I have used the spectra recorded at the highest available field strength (14.1 T) shown in fig. 2.12 on page 19 and recorded using the two-axis goniometer probe.

Figure 8.3A shows expansions of the region around the central transition of the ^{23}Na spectra resulting from rotation about the a axis. These resonances may all be fitted to gaussian line shapes with line widths ranging from 1.3 to 1.8 kHz and their centerfrequencies (ν_{res}) make excursions over a frequency range of approximately 1 kHz. Under such conditions (i.e., the line width being larger than the span of the resonances) we can not expect a very good agreement between the experimental and simulated rotation plots because of the measurement error.

Figure 8.3B shows the rotation plots for the central transition of ^{23}Na in $NaNO_3$ with the experimental resonances marked by dotted circles. A calculation of the second-order quadrupolar shift using the optimized quadrupole coupling parameters determined from analysis of the satellite transitions (table 2.2 on page 20) and optimizing the isotropic chemical shift is represented by the dashed lines in fig. 8.3B. These lines do not fit the experimental resonances convincingly. However, by intro-

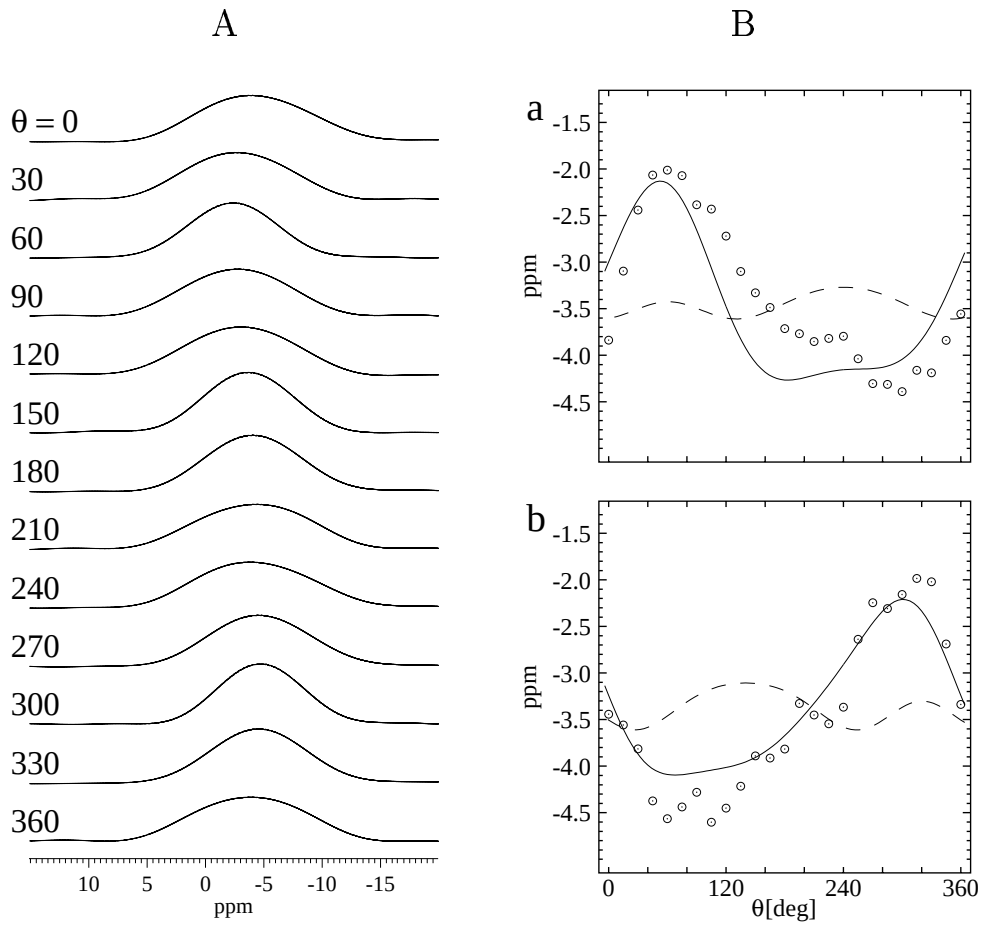

Figure 8.3: (A) Expansion of the region for the central transition of the ^{23}Na single-crystal NMR spectra of $NaNO_3$ recorded for rotation about the a axis and shown in full in fig. 2.12 on page 19. Every second spectrum is shown. (B) Rotation plots of the ^{23}Na central transition for $NaNO_3$ with the experimental resonances marked as dotted circles. The dashed lines correspond to simulations of the quadrupole coupling from table 2.2 and the optimized isotropic chemical shift. The solid lines correspond to combined effect of quadrupole coupling (parameters from table 2.2) and the CSA parameters listed in table 8.2.

ducing the CSA interaction in addition to the quadrupole coupling in simulations where the quadrupole coupling parameters are fixed at the values determined from the satellite transitions results in the parameters summarized in table 8.2. The fit between the experimental resonances and the simulated curves including the CSA (solid lines in fig. 8.3B) is definitely improved as compared to the "pure" second-order quadrupolar rotation plots, although it is not as convincing as the example of ^{27}Al CSA in α-Al_2O_3 shown in the previous section. The effect of the CSA is also reflected by the *rms* deviation between experimental and simulated rotation

Table 8.2: ^{23}Na chemical shielding parameters ($\delta_\sigma, \eta_\sigma, \delta_{\rm iso}$) and relative orientation (χ) of the V_{zz} and σ_{zz} principal elements for $NaNO_3$ determined from ^{23}Na single-crystal NMR.

ν_0 [MHz]	δ_σ [ppm]	η_σ	χ [°]	$\delta_{\rm iso}$ [ppm]	Reference
158.7	-1.6 ± 0.2	0.0 ± 0.3	8 ± 5	–	This work
11	1 ± 3	0^a	0^b	49 ± 1^c	*175*
65	0 ± 1	0^a	0^b	48 ± 1^c	*175*

[a] Axial symmetry assumed from crystal symmetry. [b] The quadrupole coupling and CSA tensors are assumed parallel from crystal symmetry. [c] Isotropic chemical shifts are relative to the free Na^+ ion.

plots. By introducing the CSA in addition to the quadrupole coupling interaction, the *rms* deviation is decreased from 136 Hz (dashed lines) to 57 Hz (solid lines).

$NaNO_3$ belongs to the trigonal space group $R\overline{3}c$ with the Na^+ ions located on the $\overline{3}$ axis parallel to the c axis. The resulting constrains ($\eta_\lambda = 0$ and $\chi = 0$) are fulfilled for the present data. This observation adds to the reliability of the ^{23}Na CSA parameters for $NaNO_3$.

^{23}Na MAS NMR of Na_2SO_4

The ^{23}Na quadrupole coupling in Na_2SO_4 is approximately one order of magnitude larger than in $NaNO_3$. Therefore a high-speed spinning ^{23}Na MAS NMR spectrum of the central transition of Na_2SO_4 shows the characteristic lineshape due to the second-order quadrupolar Hamiltonian. The ^{23}Na quadrupole coupling parameters have been determined earlier from static (*70*) and MAS (*142*) NMR.

We had the opportunity to record a series of ^{23}Na MAS NMR spectra of Na_2SO_4 at 17.6 T. This high field strength is ideal for detection of a small CSA because at the same time the spectral effect of the CSA is increased while the second-order quadrupolar broadening is decreased by increasing the magnetic field strength.

Figure 8.4a shows an experimental ^{23}Na spectrum of Na_2SO_4 recorded at 17.6 T (198.4 MHz) employing a spinning frequency of 2018 Hz.[2] A simulation of this spectrum including only the quadrupole coupling interaction is shown in fig. 8.4c. We observe a lack of intensity in the ssb's compared to the experimental spectrum, and furthermore, the line shape of the centerband differs significantly from the experimental.

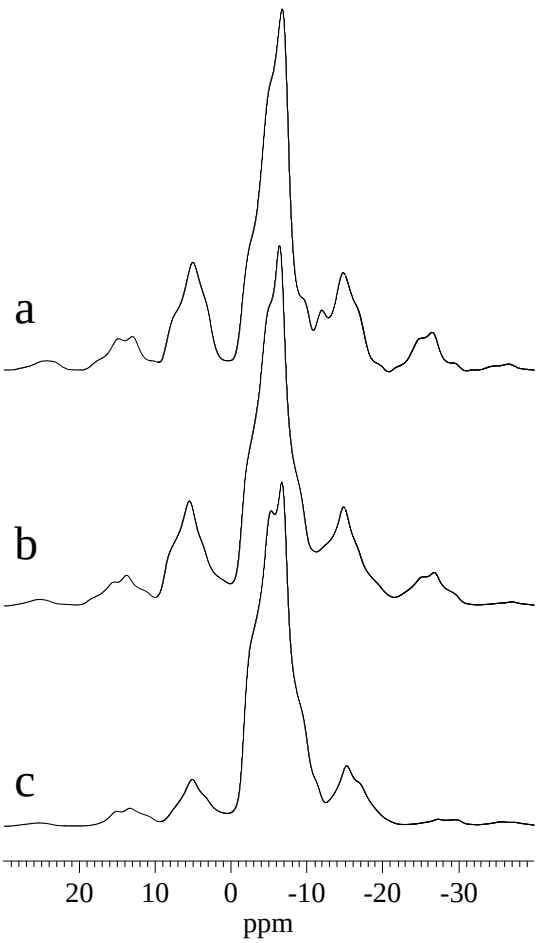

Figure 8.4: Experimental (a) and simulated (b, c) 17.6 T ^{23}Na MAS NMR spectra of Na_2SO_4 (ν_r = 2018 Hz). The simulations are performed with (b) and without (c) the CSA taken into account.

By introducing the CSA as an additional interaction we obtain the simulation shown in fig. 8.4b, and we note that this simulation not only provides the right intensity distribution in the ssb's but also exhibits the same line shape as the experimental spectrum. The resulting quadrupole coupling and CSA parameters from this optimization are listed in table 8.3 along with their error limits evaluated from the sensitivity of the simulation towards variation of the particular parameter.

We note that there is a good agreement between the present ^{23}Na quadrupole coupling parameters and those of previous static ($C_Q = 2.62 \pm 0.17$ MHz $\eta_Q = 0.6 \pm 1$ (*70*)) and MAS ($C_Q = 2.60$ MHz and $\eta_Q = 0.58$ (*142*)) NMR investigations, although the present quadrupole coupling constant is slightly smaller. This might

[2]All the ^{23}Na MAS NMR spectra of Na_2SO_4 are recorded employing single-pulse excitation ($\tau_p = 2$ μs), a spectral width of 100 kHz, and 240-320 transients with a repetition delay of 1 s.

Table 8.3: ^{23}Na quadrupole couplings (C_Q, η_Q), chemical shielding anisotropies $(\delta_\sigma, \eta_\sigma)$, and relative orientations (ψ, χ, ξ) for Na_2SO_4 determined from ^{23}Na MAS NMR at 17.6 T.

ν_r [Hz]	C_Q [MHz]	η_Q	δ_σ [ppm]	η_σ	ψ [deg]	χ [deg]	ξ [deg]
1624	2.48	0.61	−10.3	0.70	17	73	23
2018	2.49	0.61	−10.3	0.71	11	73	24
2125	2.49	0.58	−10.0	0.86	−7	69	20
2675	2.45	0.61	−11.0	0.73	25	79	21
Mean data							
	2.48 ±0.03	0.60 ±0.03	−10.4 ± 1.0	0.75 ±0.15	12 ± 20	74 ±7	22 ±10

be due to a temperature effect.[3]

Within the orthorhombic crystal structure of Na_2SO_4 (space group *Fddd*) the Na^+ ions are located in position 16(*g*) with local two-fold symmetry (*177*, *178*). Thus we expect that the Euler angles ψ, χ, ξ reflect this symmetry, and we observe that the values $\psi = \xi = 0°$ correspondong to $V_{yy} \parallel \sigma_{yy}$ is almost fulfilled within errors (table 8.3). It may be misleading to interpret the value $\xi = 22 \pm 10°$ as $\xi = 0°$. However, iterative fittings with fixed values for the two Euler angles ($\psi = \xi = 0°$) result in values for the other parameters which are within the error limits.

In conclusion, considering the two simulations in fig. 8.4 we have a convincing determination of the ^{23}Na CSA in Na_2SO_4. Although the CSA is very small we have also been able to determine the ^{23}Na CSA parameters for Na_2SO_4 from slow-speed MAS at 9.4 T (*179*).

[3]We have observed that ^{87}Rb quadrupole coupling parameters in inorganic salts are very dependent on the sample temperature. Thus even the frictional heating from the spinning may introduce small changes in the quadrupole coupling parameters (*176*).